Calcium-phosphorus interactions at a nano-structured silicate surface

Daniel C Southam[*1] and Trevor W Lewis*

AUTHOR ADDRESS School of Chemistry, University of Tasmania, Locked Bag 1371, Launceston 7250, Tasmania, Australia

Andrew J McFarlane, T Borrmann and Jim H Johnston

AUTHOR ADDRESS School of Chemical and Physical Sciences, Victoria University of Wellington, PO Box 600, Wellington 6140, New Zealand

[1] CURRENT ADDRESS Nanochemistry Research Institute, Department of Applied Chemistry, Curtin University of Technology, GPO Box U1987, Perth 6845, Western Australia, AUSTRALIA. Telephone +61-8-9266-2380 Facsimile +61-8-9266-4699 Email D.Southam@curtin.edu.au

ABSTRACT

Nano-structured calcium silicate (NCS), a highly porous material synthesized by controlled precipitation from geothermal fluids or sodium silicate solution, was developed as filler for use in paper manufacture. NCS has been shown to chemisorb orthophosphate from an aqueous solution probably obeying a Freundlich isotherm with high selectivity compared to other common environmental anions. Microanalysis of the products of chemisorption indicated there was significant change from the porous and nano-structured morphology of pristine NCS to fibrous and crystalline morphologies and non-porous detritus. X-ray diffraction analysis of the crystalline products showed it to be brushite, $CaHPO_4 \bullet 2H_2O$, while the largely x-ray amorphous component was a mixture of calcium phosphates. A two-step mechanism was proposed for the chemisorption of phosphate from an aqueous solution by NCS. The first step, which was highly dependent on pH, was thought to be desorption of hydroxide ions from the NCS surface. This was kinetically favoured at lower initial pH, where the predominant form of phosphate present was $H_2PO_4^-$, and led to decreased phosphorus uptake with increasing pH. The second step was thought to be a continuing chemisorption process after stabilization of the pH-value. The formation of brushite as the primary chemisorption product was found to be consistent with the proposed mechanism.

KEYWORDS: Nano-structured calcium silicate; phosphate sequestration; chemisorption; calcium phosphate; hydroxyapatite inhibition

GRAPHICAL ABSTRACT

A porous nano-structured calcium silicate (NCS) was shown on to produce $CaHPO_4 \bullet 2H_2O$ on exposure to phosphate. A temperature- and pH-dependent mechanism was proposed for the chemisorption of phosphate by NCS.

INTRODUCTION

Phosphorus as phosphate poses a known environmental threat in natural waters, with high nutrient concentrations leading to eutrophication of waterways by algal blooms. The fate of phosphorus in the environment is controlled through lack of a gaseous step in its cycle. Cycling of phosphorus in the environment has been accelerated by anthropogenic activities, with pre-human fluxes estimated at 2 – 3 x 10^6 tonnes-P a^{-1} compared with current river inputs estimated at 4 – 6 x 10^6 tonnes-P a^{-1} due mostly to fertilizer use, deforestation, soil erosion and urban as well as industrial effluent [1, 2]. There is a need for highly efficient and selective methods for the sequestration of phosphate from point sources of wastewater. Examples of current research on phosphate sorbents studied for environmental sequestration include the use of waste materials such as blast furnace slags [3, 4], ash from coal combustion [5-8] and paper sludge [9], metal-doped citrus processing waste [10] and red mud from bauxite processing [6]; synthetic and naturally occurring minerals and materials [11-15] and novel ion exchange materials [16-18].

A nano-structured calcium silicate material containing surface-bound calcium ions was considered as a sorbent for phosphate removal from aqueous solutions. Nano-structured calcium silicate (NCS) is a highly porous material produced by controlled precipitation from geothermal fluids or commercial silicate solutions (sodium silicate). Its current application is as filler in newsprint and specialty papers as it has very high optical brightness and whiteness and is also beneficial in reducing print-through in newsprint [19-22]. The chemical and physical properties of NCS make this a candidate for the highly efficient treatment of aqueous waste containing phosphate and other ions [19, 23]. NCS consists of nanometer-sized platelets arranged in particles between 0.5 and 20 μm in size. It has a high absorption capacity of up to 700 g-oil per 100 g NCS and a high surface area of 350 – 600 m^2 g^{-1} [21]. Two forms of NCS display especially high surface areas and pore volumes, which are interesting for sorption experiments: a spacer compound containing silicate (NCS-2EE, $Ca_{0.8}SiO_{2.8}\cdot 2H_2O$) and a Reinforced silicate (NCS-Rein, $CaSi_{1.75}O_{3.5}\cdot 3H_2O$). The treatments are necessary as the silicate structure can collapse due to strong attractive forces between calcium and silanol groups located on its surface. Treatment with a spacer-compound leaves a minimal amount

(<3 %w/w) of an organic compound coordinated to the active groups, while during reinforcement the surface bound calcium is encapsulated in silicon dioxide.

Previous research [24] has shown that nano-structured calcium silicate effectively and efficiently chemisorbs orthophosphate in all forms from aqueous solution, showing probable conformity to a Freundlich isotherm. Phosphate was found to chemisorb at several orders of magnitude above other common environmental anions, such as nitrate and chloride. The monobasic form of phosphate ($H_2PO_4^-$) was chemisorbed with higher loadings of up to 1.9 mmol-P per g-NCS, and hence greater efficiencies showing significant improvements on other sorbent-based methods for phosphorus removal. Comparison of the reaction between the three forms of phosphate and NCS showed that $H_2PO_4^-$ was favoured, with an activation energy of 39.37 kJ mol^{-1} compared to 56.71 and 61.69 kJ mol^{-1} for HPO_4^{2-} and PO_4^{3-} respectively. This was found to contradict the initial assumptions that PO_4^{3-} would be preferentially sorbed leading to formation of either hydroxyapatite (HAP, $Ca_{10}(PO_4)_6(OH)_2$) or tricalcium phosphate (TCP, $Ca_3(PO_4)_2$) due to their lower solubilities, and hence higher thermodynamic stability of the products [25].

Frossard *et al* [25] studied the precipitation of calcium phosphates on pure calcite surfaces to determine the crystallisation patterns during phosphorus uptake on calcareous soils. It was found that monocalcium phosphate (MCP, $Ca(H_2PO_4)_2$) is initially formed followed rapidly by dicalcium phosphate dihydrate (DCPD, $Ca(HPO_4)\cdot 2H_2O$) or brushite. On pure calcite surfaces this progresses to octacalcium phosphate (OCP, $Ca_8H_2(PO_4)_6\cdot 5H_2O$) and finally to HAP. However, when precipitation occurs on calcite in soils this process ceases at brushite and does not produce either OCP or HAP [25].

The termination at brushite is due to the presence of surface-bound fulvic, humic and tannic acids [26] or magnesium ions [27] inhibiting the crystallisation of OCP. Organic acids are known to both inhibit production of HAP and promote crystallisation of brushite [28]. This, in part, explains why there is a greater amount of bioavailable phosphorus in soils treated with manure or animal waste; natural organic matter prevents precipitation of insoluble apatite [25, 26, 29, 30].

Detailed chemical and morphological studies on the reaction between the surface-bound calcium

ions and phosphate in solution and the products of such a reaction were undertaken to assist in the development of a mechanism for chemisorption.

MATERIALS AND METHODS

Nanostructured calcium silicate (NCS), as proprietary to Victoria University of Wellington, New Zealand, is synthesized by acidifying a slurry of 34.6 g (0.468 mol) calcium hydroxide in 460 mL of water to a pH of 11.5 and reacting it with 87.8 g (0.420 mol) sodium silicate (Orica) in 450 mL water [19]. Geothermal silicate sources can be employed as well as long as the pH and calcium to silicate ratio are maintained. The NCS was filtered and extensively washed with water (NCS-w). Three forms of calcium silicate were prepared: an untreated calcium silicate (NCS-w), a spacer compound containing silicate (NCS-2EE) and a Reinforced calcium silicate (NCS-Rein). To incorporate a spacer compound into NCS the filter cake was washed extensively with 2-ethoxyethanol (NCS-2EE). For the Reinforcement: the filter cake is re-slurried in 1L of water (if only part of the filter cake is re-slurried, the amount of water needs to be adjusted). For every 50 mL of resulting slurry 2.8 g of additional sodium silicate solution are added under stirring followed by washing with a small amount of dilute acid, filtration and extensive washing with water (NCS-Rein). All silicates were dried at 80 °C under vacuum for 1 hour (Thermoline VORD vacuum oven connected to a Javac 8524PVH-11 vacuum pump) and stored in a desiccator over silica gel until use. Type I water (DirectQ-5, Milli-Q, Millipore, France) was used for all solutions and dilutions. Analytical grade reagents or better were used in all cases unless otherwise stated.

KINETIC STUDIES Isothermal studies of the sorption of the three common forms of phosphate ($H_2PO_4^-$, HPO_4^{2-} and PO_4^{3-}) by NCS-2EE at 2.8, 13.3, 25.3, 36.8 and 46.4 °C (± 0.1 °C) were undertaken in a purpose-built 1 L jacketed stainless steel reaction vessel. The temperature was controlled via a ducted water bath (Julabo F 26) and measured in the reaction vessel via a digital thermocouple (K-type, Digitron T206TC). The solution was mixed with a variable speed overhead stirrer (IKA Eurostar Digital at ca 400 min^{-1}) fitted with a purpose-built glass stirring-rod.

A solution of 1.00 mmol-P L^{-1} orthophosphate, as either potassium dihydrogen orthophosphate (AnalaR, BDH), potassium monohydrogen orthophosphate (AnalaR, BDH) or sodium tribasic phosphate (GPR, BDH) in Type I water, was placed in the reaction vessel and allowed to come to temperature. A known mass of NCS (ca 0.5 g) was introduced to the vessel and allowed to mix.

Aliquots of ca 10 mL were taken at regular intervals between 0 and 24 hours, filtered and analysed colourimetrically by the vanadomolybdate method as described by Greenberg *et al* [31]. The pH was monitored simultaneously via a pH electrode in the reaction vessel (Orion pH triode coupled to a 720A meter and calibrated at pH 7.00 and 10.00 with pre-prepared (commercially available) buffer solutions).

SCANNING ELECTRON MICROSCOPY Scanning electron microscopy (SEM) was used to determine changes to the surface of NCS after reaction with orthophosphate. Energy dispersive spectroscopy (EDS) was also used for qualitative analysis of the surface changes to the NCS after exposure to orthophosphate [32].

The reaction between NCS (NCS-2EE or NCS-Rein, ca 0.5 g) and a solution of potassium dihydrogen orthophosphate (AnalaR, BDH, 0.100 mol L^{-1}) was undertaken as above. The NCS was filtered from the mother liquor, a portion was rinsed in water and another in 2-ethoxyethanol and the samples dried in an oven at 110 °C for 24 hours.

The four samples and a sample of pristine NCS were mounted using double-sided adhesive tape on aluminium SEM stubs and sputter-coated with gold (Bal-tec SCD-050) for the samples used for imaging, or evaporative coated with carbon (Ladd Research Industries) for EDS analysis to prevent the overlap between the gold and phosphorus K peaks.

SEM was undertaken with an Electroscan Environmental Scanning Electron Microscope (ESEM) 2020 in scanning mode at 15 kV under high vacuum. Energy Dispersive Spectroscopy (EDS) was undertaken using an Oxford LinkPentafet EDS attached to the above ESEM instrument. For all SEM studies the full width of the scale bar on the micrograph represents the width stated.

POWDER X-RAY DIFFRACTION Powder x-ray diffraction (XRD) patterns were collected for phase analysis of the residues analysed by SEM above. Random powder samples were prepared by hand grinding in a mortar and pestle and the diffraction patterns were acquired between 5 and 65 ° 2θ on a Siemens D500 Bragg-Brentano Diffractometer operated at 40 kV and 40 mA using Cu-K_α radiation. The step size was 0.02 ° 2θ with a scan rate of 0.4 ° 2θ per minute. MDI–Jade (version 6) automated phase identification software was used to analyse the diffraction patterns.

X-RAY CRYSTALLOGRAPHY Single crystal x-ray crystallography was used to capture the diffraction pattern of a crystal and return dimensions of its unit cell. Each crystalline species has a unique unit cell dimension, which gives each a “fingerprint” for confirmation of identity.

NCS was pressed in a pelletiser (Specac 15.010) at 10T pressure. A section of the subsequent disc was placed in a scintillation vial containing 0.1 mol P L^{-1} as $H_2PO_4^-$ and crystals allowed to grow. The crystals were left for a 6-month period to obtain suitably sized samples for x-ray crystallographic analysis.

Single crystal x-ray crystallography was undertaken on a sample mounted under argon in a glass capillary with epoxy resin (Araldite, Selleys Australia). Cell determinations and data acquisitions were carried out using an Enraf-Nonius turbo CAD4 diffractometer with a graphite single crystal monochromated molybdenum radiation source, assumed to be 0.71073 Å (K_α) at 298 K. The unit cell calibration was performed using 25 reflections well separated in reciprocal space.

RESULTS AND DISCUSSION

KINETICS Isothermal studies were used to extend the loading studies previously described [24] and to provide information about the mechanism of sorption. As two chemical quantities were monitored during the reaction two sets of kinetics are presented: firstly with respect to the loss of phosphate from the solution and secondly with respect to hydrogen ion concentration as determined from pH. Typical plots of phosphate loading and pH versus time are given in Figure 1.

The kinetics of the chemisorption of the various forms of orthophosphate by NCS was determined for first order [1] and second order [2], where $x = 0, 1, 2$; t = time of sampling and k = rate constant. The reaction between NCS and three forms of orthophosphate ($H_2PO_4^-$, HPO_4^{2-} and PO_4^{3-}) at an initial concentration of 1.00 mmol-P L^{-1} was undertaken at five temperatures between 2.8 °C and 46.4 °C. NCS showed a general trend for all forms of orthophosphate, with increased uptake of phosphate at decreased initial pH. The kinetics using the same rate equations with respect to hydrogen ion concentration is presented and discussed later.

$$\ln\left(\frac{[H_xPO_4^{(3-x)-}]_t}{[H_xPO_4^{(3-x)-}]_0}\right) = -kt \qquad 1$$

$$\frac{1}{[H_xPO_4^{(3-x)-}]_t} = kt + \frac{1}{[H_xPO_4^{(3-x)-}]_0} \qquad 2$$

At higher temperatures the reaction between orthophosphate and NCS was found to be entirely second order. For example in Figure 2(a) the reaction between monohydrogen orthophosphate and NCS at 36.8 and 46.4 °C exhibited consistent linearity for the second order plot. A comparison of the first and second order plots for the reaction for the same reaction conditions as in Figure 2(a) but at 2.8 °C is given in Figure 2(b). At both lower temperatures and higher initial pH there were two distinct linear regions, which indicated a two-step process was occurring. It was found that both steps were affected by initial pH and temperature. This clearly shows a dependence on the temperature for the appearance of a discernable first step, which was totally lacking at the higher temperatures in Figure 2(a). At lower initial pHs, and hence a predominantly different form of phosphate, the first step was also apparent. To differentiate between the two steps each first and

second order plot was split into two regions. The first step was found to occur in the majority of experiments in the first thirty minutes, with the second step occurring in the remaining time period.

The occurrence of this first step made the resolution of the order of both steps difficult. However, with the confirmation of a second order process at higher temperatures, it was likely that the second step at lower temperatures was also second order as it occurred over an increasing portion of the time range at higher temperature. Comparison of linearity of the first and second order linear plots for both steps was undertaken to confirm the order of each step. The difference between the second and first order squared-residual values from ordinary least squares regression strongly indicated that the second step was second order with respect to phosphate.

The resolution of the order of the first step was more difficult, as there was evidence for both first and second order processes with respect to phosphate. While the overall fit to a second order process was moderately apparent, indisputable evidence was not provided by this data. This was likely due to the sparsity or uncertainty of data in this region. As such it is concluded the initial step is also second order with respect to phosphate.

The reaction between NCS and all forms of phosphate has been shown to cause a change in pH, see Figure 1, which mirrors the change in phosphate concentration. The pH in most cases was found to tend to a common value, regardless of the initial pH, of between 9 and 11. For the kinetics experiments the pH was measured *in situ* and the results for the same experiments under the same conditions and at approximate times as for the phosphate data. The same trends between forms of phosphate and pH change seen in the loading studies were exhibited at all temperatures in the kinetics studies.

The same two-step process as with respect to phosphate was clearly evident with respect to hydrogen ions. In the reaction between NCS and $H_2PO_4^-$ or HPO_4^{2-} the reaction was found to be highly dependent on temperature, with the initial step, which was clearly second order, seen at all temperatures.

For example in Figure 3 for the reaction between NCS and $H_2PO_4^-$ at 2.8, 25.0 and 46.4 °C the rate of the first step was found to decrease and its duration to increase with decreasing temperature. The

presence of a second order first step, with respect to hydrogen ion concentration, supported the hypothesis above where the first step was found to be a second order process with respect to phosphate. The likely mechanism for the first step for both $H_2PO_4^-$ and HPO_4^{2-} was an acid/base reaction.

The second step in the reaction between $H_2PO_4^-$ or HPO_4^{2-} and NCS was found to be independent of hydrogen ion concentration. For both the first and second order plots of these reactions at all temperatures the slope of the graph was found to be consistently around zero. This indicated a zero order process for the second step with respect to hydrogen ion concentration.

In the case of the reaction between PO_4^{3-} and NCS there was no consistent, discernable division of the reaction into two steps. No conclusions about the order of the reaction between PO_4^{3-} and NCS with respect to hydrogen could be made. To place the results for PO_4^{3-} in context, direct comparison to the results for reaction with $H_2PO_4^-$ were made. In all cases the slope was found to be approximately 0, and was not even of the same magnitude as the first and second order plots for $H_2PO_4^-$ as the initial form of phosphate present under the same conditions.

From this the reaction between PO_4^{3-} and NCS was determined to be zero order with respect to hydrogen ion concentration. This was in good agreement with the assumption that at lower initial pH an initial, pH dependent, acid/base reaction occurred in the first step. At higher initial pH the lack of available hydrogen ions from the phosphate saw a decrease in the prevalence of this step, and dependence on hydrogen ion concentration. This subsequently led to slower, kinetically unfavoured reactions with increasing initial pH, inhibited by the absence of hydrogen ions.

MICROSTRUCTURE Nanostructured calcium silicate has been shown by Johnston *et al* [19, 21, 22] to be a material of high porosity, with nanometre-sized pores in an open framework arrangement, and exhibiting a “desert rose” type surface morphology. Three forms of NCS from the same batch, but with differing post-treatments, were analysed. They all exhibited similar physical properties, with very bright, white colour, low density and no apparent crystallinity. As can be seen in Figure 4 the described desert rose microstructure and high porosity were clearly visible. Microstructural analysis by SEM of the pore size in Figure 4 indicated that the pores averaged between 100 and 500 nm in

diameter around a larger open framework of ca. 1 μm in diameter. The average of several energy dispersive spectroscopy (EDS) spot analyses of the unreacted NCS was taken, showing the presence of silicon, calcium and oxygen in the specimens with a small sodium K line also observed, indicating incomplete washing of the product after precipitation.

After reaction between NCS and 0.1 mol P L^{-1} as $H_2PO_4^-$ at 25 °C for twenty-four hours there was a profound change in the morphology of the NCS. As seen in Figure 4, there was little apparent crystallinity and definite porosity in the pristine NCS. There were three distinct morphologies identified from microstructural analysis by SEM: Firstly, detritus with little consistent morphology was present in all specimens. It appeared to retain some of the gross morphology of the pristine NCS but, from SEM analysis, no apparent porosity making it related to a collapsed form of water washed silicate (NCS-w). Secondly, fine fibres were present in all except the completely crystalline specimen and these ranged from a minor to major component of the mix. Finally, most specimens exhibited some crystallites, with some specimens were almost entirely crystalline.

The detritus exhibited a strong phosphorus line when compared with the pristine starting material, indicating that the detritus was a product of the reaction between NCS and phosphate, and not simply a collapse of the pore structure. This morphology is probably derived from the pristine NCS. The porosity seen in the pristine NCS was totally lost as can be seen in Figure 5. This loss of porosity may be due to a number of factors such as crystalline products forming in the NCS pores and collapse of the structure during treatment as described in the literature [19, 23]. The detritus material was potentially a precursor to other crystalline forms of the product, such as the fibrous morphology, formed by its dissolution and crystallization. It was not found in specimens in the absence of one or both of the other product morphologies.

Fibres (see Figure 6) were found in most specimens and were usually associated with detritus, shown as nodules on the fibres themselves (Figure 6(b)). This indicates that the fibrous crystal growth occurred from the pores of the NCS. The fibres were of considerable length in comparison to diameter (length $\approx$ 10 and 100 μm, diameter $\approx$ 250 nm and 2 μm).

The energy dispersive spectrum for the fibres showed significant silicon and oxygen lines with

reduced calcium and phosphorus lines when compared to the detritus. Comparison of the line heights of silicon and calcium for the pristine NCS (Si/Ca = 2.1), detritus (Si/Ca = 1.8) and fibres (Si/Ca = 5) illustrates the enrichment in silicon through loss of calcium in the fibres. This loss of calcium is most probably attributable to the formation of other calcium phosphate products. The crystallites were found to be almost entirely calcium, phosphorus and oxygen, with a small amount of silicon likely due to the surrounding detritus.

All specimens prepared for microstructural analysis exhibited crystallinity with clearly identifiable crystallites of between 50 to 500 μm surrounded by detritus (eg Figure 7). It is assumed that the reaction with phosphate destroyed the NCS and that calcium phosphates were the likely predominant product. Compared to the fibres the detritus did not appear to be part of these crystals. In Figure 7 the detritus was found to be sitting on, rather than included in, the crystal. This further indicated that NCS was destroyed in this process leading to formation of large crystals.

X-RAY ANALYSIS X-ray diffraction was undertaken on random bulk powder samples of pristine NCS and NCS after reaction with phosphate that was found from electron microscopy to contain predominantly a mixture of detritus and fibrous products or a mixture of detritus and crystalline products. Single crystal analysis was also undertaken to confirm the identity of the final crystalline product.

The powder diffraction (see Figure 8(a)) showed that the pristine NCS diffracted poorly and showed some broad crystalline calcium silicate peaks (**6** = Ca_2SiO_4/ $Ca_{1.5}SiO_{3.5}{\cdot}H_2O$, **7** = $Ca_{1.5}SiO_{3.5}{\cdot}H_2O$, **8** = $Na_2Ca_3Si_2O_8$ indicating impurities or micro-crystallinity) on an amorphous halo between 15 and 40 ° 2-theta. By comparison the products after reaction varied considerably in their phase composition.

Where detritus and fibrous morphologies existed the diffraction pattern (see Figure 8(b)) exhibited a mixture of residual calcium silicate peaks (**6**) and product calcium phosphate peaks. The confirmation of phase identities in the product peaks is difficult, as many calcium phosphates diffract similarly and a convoluted pattern is evident. Brushite or $CaHPO_4{\cdot}2H_2O$ (**1**) and $Ca_9HPO_4(PO_4)_5OH$ (**4**) are clearly discernable. Other potential products for the peaks identified are

$Ca_5(PO_4)_3OH$ and/or $Ca_3(PO_4)_2{\cdot}2H_2O$ (**2**) and $Ca_9HPO_4(PO_4)_5OH$ and/or $Ca_5(PO_4)_3OH$ (**3**).

The predominantly crystalline product (see Figure 8(c)) was found to diffract well and provide a strong brushite or $CaHPO_4{\cdot}2H_2O$ pattern (**1**). Examination of the crystalline material under an optical microscope identified two main morphological types; longer rods and flatter and wider plates. Each of these crystals was mounted as described and an initial single-crystal diffraction attempted. It was found that the rod crystals gave a better diffraction, and were used for the unit cell determination.

The x-ray crystallography undertaken on the sample indicated two possibilities for the unit cell with the choice of unit cell was ambiguous on initial analysis. Further analysis confirmed that the cell was monoclinic, the stoichiometry of metal centre to ligand was 1:1 and the unit cell dimensions closely matched that of brushite, $CaHPO_4{\cdot}2H_2O$. The comparison of the unit cell dimensions (see Table 1) for the references available against the experimental results show the unit cell dimension obtained matches that of brushite within experimental error.

Curry and Jones [33] obtained the unit cell from neutron activation analysis and assigned brushite to a non-uniform space group, *Ia*. Sainz-Díaz *et al* [34] transformed it to the standard space group *Cc*, and the unit cell dimensions given here represent this transformation. Sainz-Díaz *et al* obtained the unit cell dimensions from first principle calculations at 300 and 380 eV.

MECHANISM A mechanism for the reaction between NCS and phosphate is proposed from the kinetics data with respect to phosphate and hydrogen, the resolution of product morphologies from SEM and the identity of crystalline products from x-ray diffraction. Two mechanisms are proposed: one at an initial pH in the reaction liquor of between 4 and 9 where the form of phosphate present is predominantly in the $H_2PO_4^-$ and HPO_4^{2-} forms, and a second mechanism is proposed for an initial pH greater than 9 where the form of phosphate is mostly PO_4^{3-}.

Where the form of phosphate is predominantly $H_2PO_4^-$ or HPO_4^{2-} the added protonation available from the phosphate led to the kinetically favoured mechanism [3]. It is proposed from the hydrogen and phosphate kinetic data that the lower initial pH caused a rapid increase of solution pH by desorption of hydroxide ions from the NCS surface. This saw subsequent alteration of the form of

phosphate present to predominantly HPO_4^{2-} and PO_4^{3-}.

$$NCS(OH)_2 + H_xPO_4^{(3-x)-} \underset{}{\overset{k_1}{\rightleftharpoons}} NCS^{2+} + HPO_4^{2-} \xrightarrow{k_2} NCS(HPO_4) \qquad 3$$

The second step in the mechanism saw chemisorption of the phosphate by NCS, most likely as HPO_4^{2-} or PO_4^{3-} from the pH of the reaction liquor after 20 hours of between 9 and 10. The chemisorption process was also thought to have occurred during the first step, as the majority of phosphate loss was seen in this region. There was still significant phosphate loss after the equilibration of pH, and as such chemisorption was thought to occur across the full time range.

When the initial pH was high, and hence the predominant form of phosphate was PO_4^{3-}, a different mechanism occurred [4]. The lack of protonation saw a different first step, not kinetically favoured.

$$3NCS(OH)_2 \underset{}{\overset{k_1}{\rightleftharpoons}} 3NCS^{2+} + 2PO_4^{3-} \xrightarrow{k_2} NCS_3(PO_4)_2 \qquad 4$$

The ligand exchange of hydroxide for phosphate was inhibited by the already high pH. The initial lowering of the pH-value seen in loading studies for the reaction between PO_4^{3-} and NCS, for example Figure 1, was thought to be attributable to phosphate chemisorption in the second step. The chemisorption could occur on the NCS surface (detritus) or between the calcium ions released by the silicate into solution and the phosphate (fibres and crystallites).

The second chemisorption step was thought to be common to both mechanisms. This indicated that both mechanisms were likely to have occurred with reactions commencing at lower initial pH, hence leading to the kinetically favoured uptake of $H_2PO_4^-$ and HPO_4^{2-} over PO_4^{3-}.

SUMMARY

It was found that the chemisorption process between NCS and phosphate was a two-step mechanism. Both steps were found to be second order with respect to phosphate. The first step was a desorption process, most likely of surface bound hydroxide ions, during the first 30 minutes and was highly dependent on temperature and the initial pH of the reaction liquor. The second step was the true chemisorption process driven by ligand exchange, most probably by hydroxide, and hence the initial pH of the phosphate solution played a large part.

Analysis of the pristine NCS confirmed the reported microstructure and porosity of the NCS. Clearly identifiable pores of between 100 and 500 nm and an open framework pore structure were found with an apparent "desert rose" microstructure observed. EDS confirmed that the major elements present in the pristine NCS were silicon, calcium and oxygen.

Microstructural analysis of the NCS after exposure to phosphate illustrated three unique morphologies in the products, detritus, fibres and crystallites, in varying quantities between different treatments and different forms of NCS. Detritus morphology was found to exist in all specimens analysed after treatment. It was found to be a combination of residual NCS with calcium phosphate products of varying and complex structures and with little or no porosity. The fibres were found to be approximately 10 to 100 μm in length and 250 nm to 2 μm in diameter. There were also residual nodules of detritus material occurring with the fibres, which strongly indicated their occurrence was associated. Elemental confirmed the presence of silicon, calcium, oxygen and phosphorus. Crystallites were found after most sample treatments of varying size between 50 and 500 μm with residual detritus surrounding the crystals. X-ray powder diffraction identified the crystalline product as brushite, $CaHPO_4 \cdot 2H_2O$. The crystals grown from NCS exposed to a phosphate solution exhibited two types, needle or rod-like and plate-like crystals. X-ray crystallography of the crystals returned a monoclinic unit cell of a = 6.366, b = 15.181, c = 5.808 Å and β = 118.4 °, which is within experimental error of the unit cell for brushite.

It was found that the formation of less soluble and more thermodynamically stable calcium

phosphates, such as OCP and HAP, were inhibited by the presence of silicon in the NCS. The main mechanistic impetus for the kinetically favoured chemisorption of phosphate by NCS where the initial pH was lower was two-fold: through hydroxide desorption from the surface of the NCS causing a rapid kinetically favoured increase in pH and through crystallisation of brushite and subsequent inhibition of HAP formation seeing greater stability of the product at lower initial pH.

ACKNOWLEDGMENTS

This research was supported by a Tasmanian Research Scholarship (Daniel Southam) funded by the Tasmanian Government. The authors' thanks go to Dr Michael Gardiner, School of Chemistry, University of Tasmania for assistance with x-ray crystallography. Thanks also to Dr David Steele, Central Science Laboratory, University of Tasmania for assistance with SEM-EDS.

REFERENCES

1. G. M. Filippelli, in: *Phosphates: Geochemical, Geobiological and Materials Importance*, M. J. Kohn; J. Rakovan; J. M. Hughes, (Eds.) Mineralogical Society of America: Washington, DC, 2002; Vol. 48.

2. H. Tiessen, in: *Phosphorus in the global environment: transfers, cycles and management*, H. Tiessen, (Ed.) J.W.Wiley and Sons: Chichester, NY, 1995; Vol. 54, pp 1-6.

3. A. Hedstrom; L. Rastas, *Journal of Environmental Engineering (Reston, VA, United States)* **2006,** 132, (11), 1431-1438.

4. B. Kostura; H. Kulveitova; J. Lesko, *Water Research* **2005,** 39, (9), 1795-1802.

5. J. Chen; H. Kong; D. Wu; X. Chen; D. Zhang; Z. Sun, *Journal of Hazardous Materials* **2007,** 139, (2), 293-300.

6. Y. Li; C. Liu; Z. Luan; X. Peng; C. Zhu; Z. Chen; Z. Zhang; J. Fan; Z. Jia, *Journal of Hazardous Materials* **2006,** 137, (1), 374-383.

7. E. Oguz, *Colloids and Surfaces, A: Physicochemical and Engineering Aspects* **2005,** 262, (1-3), 113-117.

8. J. Yan; D. W. Kirk; C. Q. Jia; X. Liu, *Journal of Hazardous Materials* **2007,** 148, (1-2), 395-401.

9. K. Okada; Y. Ono; Y. Kameshima; A. Nakajima; K. J. D. MacKenzie, *Journal of Hazardous Materials* **2007,** 141, (3), 622-629.

10. B. K. Biswas; K. Inoue; K. N. Ghimire; S. Ohta; H. Harada; K. Ohto; H. Kawakita, *Journal of Colloid and Interface Science* **2007,** 312, (2), 214-223.

11. K. Adam; A. K. Sovik; T. Krogstad, *Water Research* **2006,** 40, (6), 1143-1154.

12. E. A. Deliyanni; E. N. Peleka; N. K. Lazaridis, *Separation and Purification Technology* **2007,** 52, (3), 478-486.

13. M. Khadhraoui; T. Watanabe; M. Kuroda, *Water Research* **2002,** 36, (15), 3711-3718.

14. E. W. Shin; J. S. Han; M. Jang; S.-H. Min; J. K. Park; R. M. Rowell, *Environmental Science and Technology* **2004,** 38, (3), 912-917.

15. S. Tanada; M. Kabayama; N. Kawasaki; T. Sakiyama; T. Nakamura; M. Araki; T. Tamura, *Journal of Colloid and Interface Science* **2003,** 257, (1), 135-140.

16. L. M. Blaney; S. Cinar; A. K. SenGupta, *Water Research* **2007,** 41, (7), 1603-1613.

17. N. I. Chubar; V. A. Kanibolotskyy; V. V. Strelko; G. G. Gallios; V. F. Samanidou; T. O. Shaposhnikova; V. G. Milgrandt; I. Z. Zhuravlev, *Colloids and Surfaces, A: Physicochemical and Engineering Aspects* **2005,** 255, (1-3), 55-63.

18. R. X. Liu; J. L. Guo; H. X. Tang, *Journal of Colloid and Interface Science* **2002,** 248, (2), 268-274.

19. J. H. Johnston; A. J. McFarlane; T. Borrmann Nano-structured Silicate, Functionalised Forms Thereof, Preparation and Uses, NZ Patent Specification No. 537747, 2005, PCT Application PCT/NZ2006/000003, 2006. 5595717.

20. R. T. Harper; I. A. Thain; J. H. Johnston, *Geothermics* **1992,** 21, (5-6), 641-51.

21. J. H. Johnston; A. J. McFarlane; T. Borrmann, *Appita Annual Conference Proceedings* **2002,** 56th, 453-457.

22. J. H. Johnston; A. J. Mcfarlane; T. Borrmann; J. Moraes, *Current Applied Physics* **2004,** 4, (2-4), 411-414.

23. M. J. Cairns; T. Borrmann; W. H. Holl; J. H. Johnston, *Microporous and Mesoporous Materials* **2006,** 95, (1-3), 126-134.

24. D. C. Southam; T. W. Lewis; A. J. McFarlane; J. H. Johnston, *Current Applied Physics* **2004,** 4, (2-4), 355-358.

25. E. Frossard; M. Brossard; M. J. Hedley; A. Metherell, in: *Phosphorus in the global environment: transfers, cycles and management*, H. Tiessen, (Ed.) J.W.Wiley and Sons: Chichester, NY, 1995; Vol. 54, pp 107-138.

26. W. P. Inskeep; J. C. Silvertooth, *Soil Science Society of America Journal* **1988,** 52, 941-946.

27. Z. Amjad; P. G. Koutsoukos; G. H. Nancollas, *Journal of Colloid and Interface Science* **1984,** 101, (1), 250-256.

28. P. R. Grossl; W. P. Inskeep, *Soil Science Society of America Journal* **1991,** 55, 670-675.

29. R. B. Harrison; F. Adams, *Soil Science Society of America Journal* **1987,** 51, 963-969.

30. G. A. O'Connor; K. L. Knudsten; G. A. Connell, *Journal of Environmental Quality* **1986,** 15, 308-312.

31. A. E. Greenberg; L. S. Clesceri; A. D. Eaton, *Standard methods for the examination of water and waste water*. 18th ed.; APHA-AWWA-WPCF: Washington, DC, 1992.

32. P. M. Cooke, *Analytical Chemistry* **1998,** 70, (12), 385R-423R.

33. N. A. Curry; D. W. Jones, *Journal of the Chemical Society A: Inorganic, Physical, Theoretical* **1971**, (23), 3725-9.

34. C. I. Sainz-Díaz; A. Villacampa; F. Otálora, *American Mineralogist* **2004,** 89, (2-3), 307-313.

FIGURES

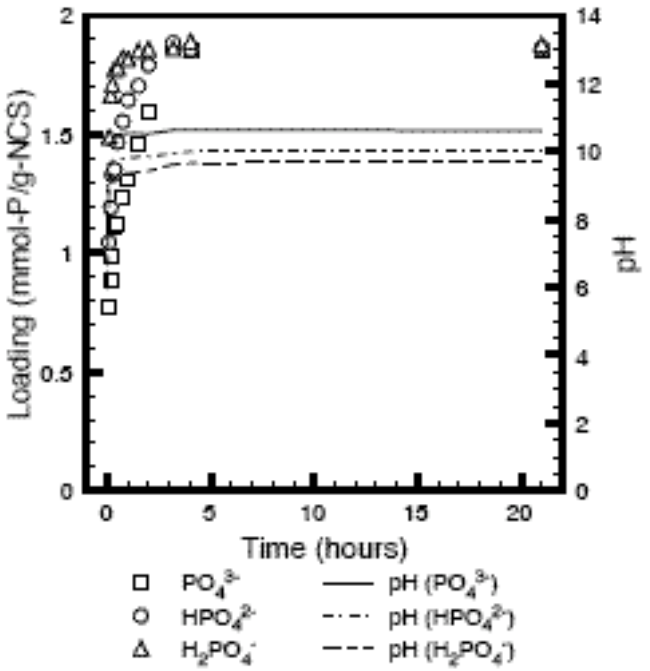

Figure 1 Comparison of loading and pH versus time for three different forms of phosphate at 46.4 °C

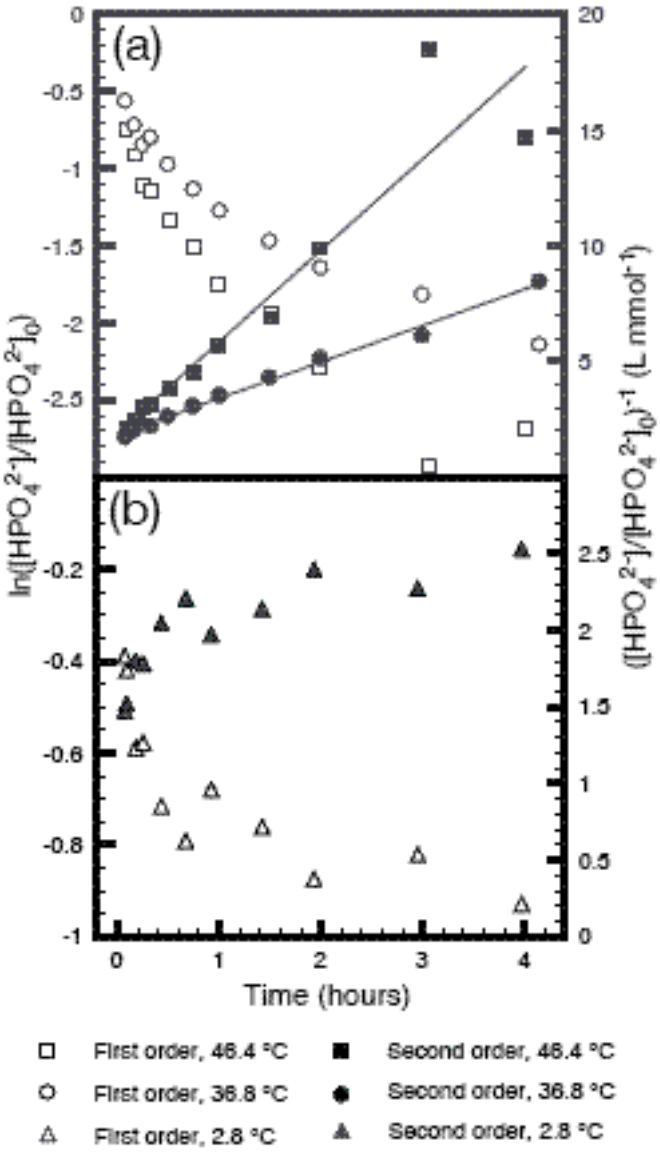

Figure 2 First and Second Order Plots with respect to phosphate for the reaction between NCS and HPO_4^{2-} at (a) 36.8 and 46.4 °C and (b) 2.8 °C

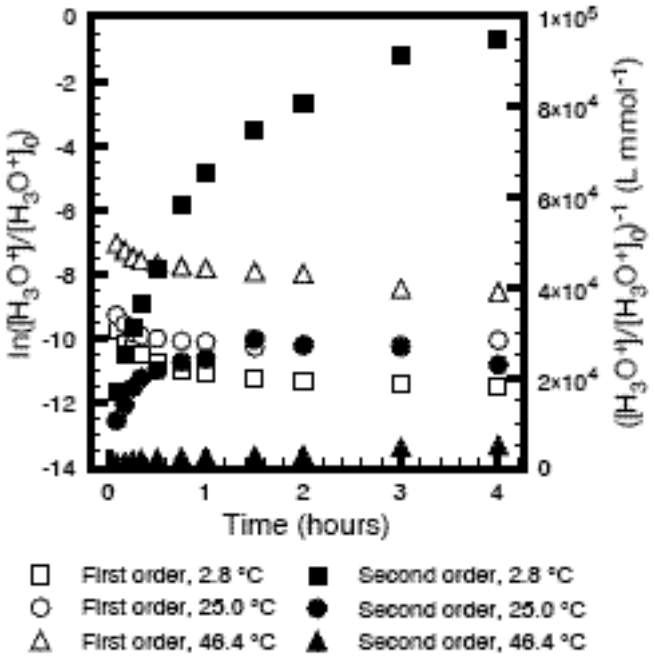

Figure 3 First and second order plots with respect to hydrogen ion concentration for the reaction between NCS and $H_2PO_4^-$

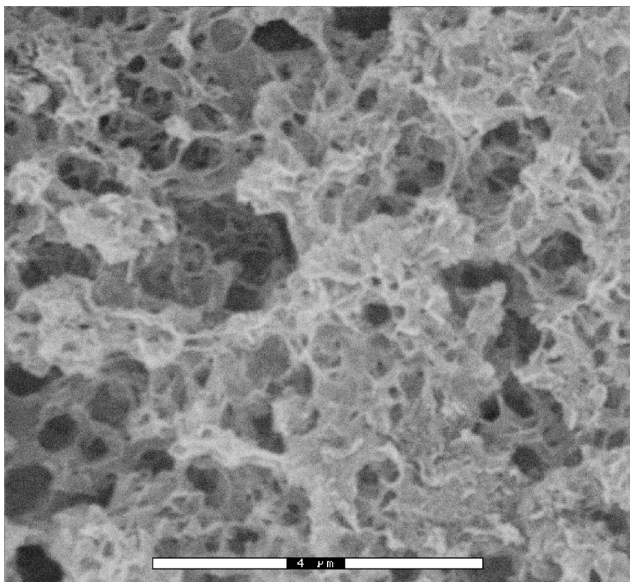

Figure 4 Scanning electron micrograph of pristine NCS (NCS-2EE)

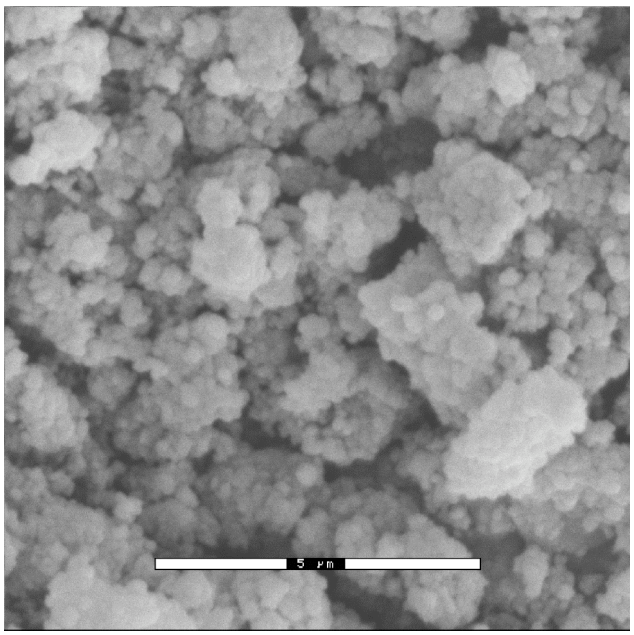

Figure 5 Scanning electron micrograph of NCS (NCS-Rein) after reaction with 0.1 M $H_2PO_4^-$ for 24 hours at 25 °C

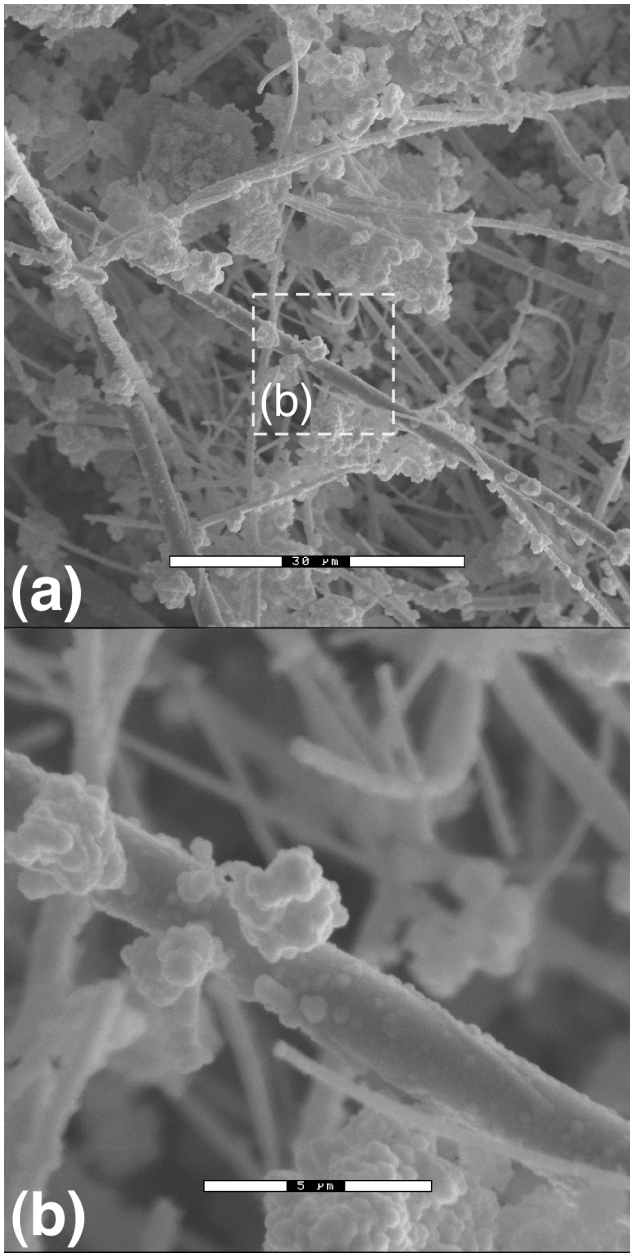

Figure 6 Scanning electron micrographs of NCS (NCS-2EE) after reaction with 0.1 M $H_2PO_4^-$ for 24 hours at 25 °C at increasing magnification

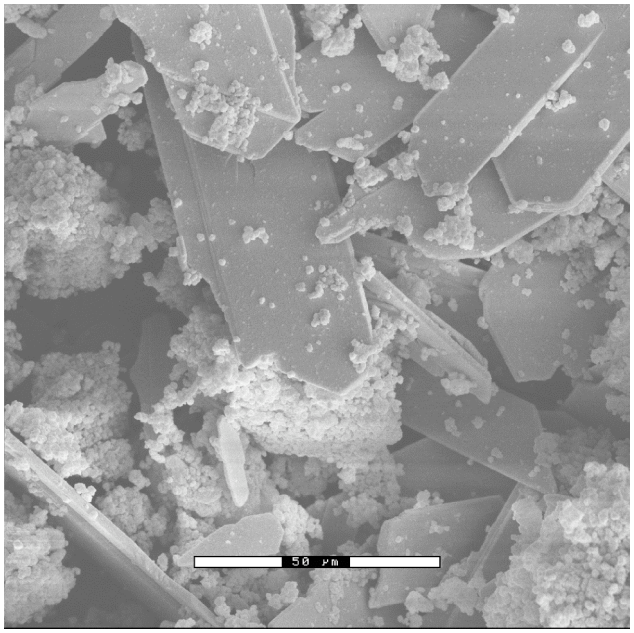

Figure 7 Scanning electron micrograph of NCS (NCS-2EE) after reaction with 0.1 M $H_2PO_4^-$ showing well formed crystals

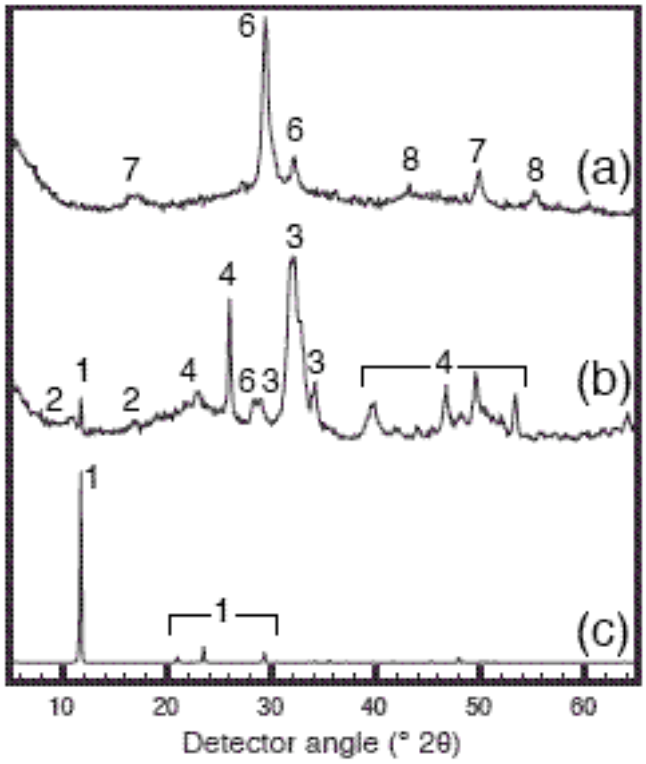

Figure 8 X-ray diffraction pattern of (a) pristine NCS and NCS after reaction with 0.1 M $H_2PO_4^-$ for 24 hours of predominantly (b) detritus and (c) crystalline material